Article

Near-Infrared-Responsive Choline-Calix[4]arene-Gold Nanostructures for Potential Photothermal Cancer Treatment

Grazia M. L. Consoli,* Giuseppe Forte, Ludovica Maugeri, Valeria Consoli, Valeria Sorrenti, Luca Vanella, Gianpiero Buscarino, Simonpietro Agnello, Massimo Camarda, Giuseppe Granata, Loredana Ferreri, and Salvatore Petralia*

Cite This: *ACS Appl. Nano Mater.* 2023, 6, 358–369

Read Online

ACCESS | 📊 Metrics & More | 📖 Article Recommendations | 🗊 Supporting Information

ABSTRACT: The development of novel chemical approaches for the fabrication of gold nanostructures with localized surface plasmon resonance (LSPR) falling in the near-infrared (NIR) region is one challenging topic in nanomaterials science. Due to their optical and photothermal properties triggered by light excitation in the therapeutic window (λ_{max} = 650−1300 nm), gold-based nanostructures are appealing candidates in anticancer nanomedicine. Here, we report a novel method to prepare water-dispersible gold nanostructures with NIR-LSPR (λ_{max} = 600−1000 nm) properties. The gold nanostructures were achieved in a single step by an unconventional method using NADH as a reducing agent and an amphiphilic choline-calix[4]arene derivative (Chol-Calix) forming micelles as a template. The CholCalix-Au nanostructures were characterized by UV−visible spectrophotometry, Raman spectroscopy, and atomic force microscopy. Agglomeration of the nanostructures due to multiple crosslinking interactions was observed and supported by modeling simulation. Effective anticancer photothermal-induced effect of the CholCalix-AuNPs was demonstrated on human breast cancer cells irradiated with biofriendly light at 808 nm.

KEYWORDS: *gold nanostructures, calixarene, photothermal effect, molecular modeling, photothermal therapy, cancer treatment*
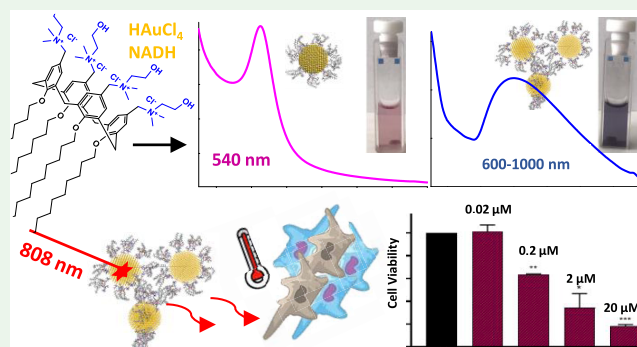
INTRODUCTION

Nanotechnology is an emerging strategy for more effective cancer treatment.[1] A nanostructure offers the benefit of especially accumulating in cancer tissues by exploiting the leaky nature of the tumor vasculature (enhanced permeability and retention effect)[2] or by binding receptors overexpressed on cancer cells (targeted anticancer therapy).[3] The anticancer activity preferentially localized in the desired sites of therapeutic action can improve therapeutic efficacy while decreasing the deleterious side effects of current chemotherapy. Use of stimuli-responsive nanostructures constitutes a more advanced approach for more effective and safer cancer treatment.[4] Nanostructures activated by extracorporeal or endogenous stimuli (i.e., light, temperature, pH, hypoxia) allow for excellent spatiotemporal- and dosage-controlled anticancer activity.

Photothermal therapy (PTT) is one of the most promising cancer treatments.[5] It consists of local generation of heat by irradiation of photoresponsive structures. Several studies have shown that mild hyperthermia (41−47 °C for 10 min) mediated by functional nanomaterials selectively destroys cancer cells because of their reduced heat tolerance compared to normal cells. Mild-PTT induces tumor destruction and cell death by loosening cell membranes and denaturing proteins[6] as well as by disrupting mitochondria, causing cancer cell death,[7] or stimulating tumor-specific innate and adaptive immune responses for tumor control.[8]

Gold-based nanostructures are the main mediators of PTT as gold nanoparticles (AuNPs) offer good biocompatibility, effective photothermal conversion upon visible or near-infrared (NIR) light absorption due to the localized surface plasmon resonance (LSPR) phenomenon, and tunability of optothermal and biotargeting properties by ease of synthetic modifications.[9,10]

Hybrid nanomaterials that combine the unique physical and chemical properties of two or more classes of nanomaterials also hold great promise for cancer diagnosis and therapy.[11] The combination with carbon-based molecules is an important
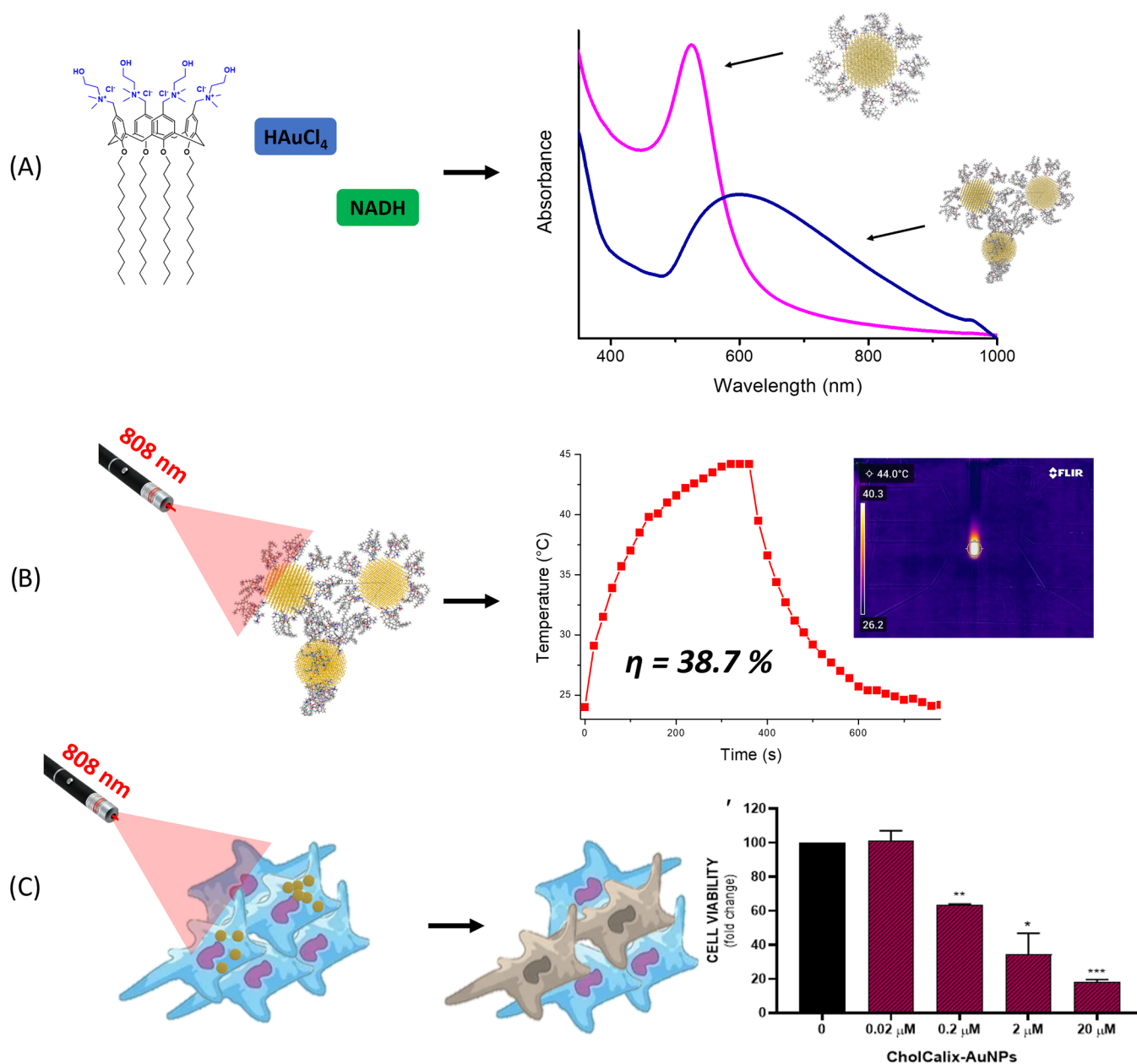
Scheme 1. Schematic Illustration of: (A) Preparation of CholCalix-AuNP and CholCalix-AuNP Clusters; (B) Laser Irradiation of CholCalix-AuNPs (808 nm) and Photothermal Conversion; (C) Cell Vitality Reduction of Human Breast Cancer Cells Treated with CholCalix-AuNPs and Irradiated with Laser 808 nm

key to equipping AuNPs with features mandatory for their application in PTT such as chemical and colloidal stabilities, dispersibility in physiological conditions, stability upon pulsed-laser irradiation, and specific binding to cancer cells by decoration with targeting ligands.[12−14] For these reasons, gold nanoparticles have been coated with a large variety of carbon-based compounds (peptides,[15] proteins,[16] DNA,[17] polymers,[18] etc.), including calix[n]arenes.

Calix[n]arenes are a family of polyphenolic macrocycles that, due to their ease of modification, have provided a large number of structures for biomedical applications,[19] including cancer treatment.[20] An intense research activity deals with innovative stimuli-responsive calixarene derivatives promoting tumor accumulation of anticancer drugs[21] and targeted cancer cell drug delivery.[22] Calixarene-based nanocarriers have also been proposed for photodynamic therapy (PDT),[23,24] photo-

theranostics,[25] and PTT. Recently, Guo et al. reported a supramolecular formulation of a hypoxia-responsive calixarene derivative and an IR780 dye for effective imaging-guided PTT.[26]

Due to the unique architecture and chemical modification possibilities, calixarene macrocycles have received a lot of attention from the scientific community as agents for coating of AuNPs. The combination with the calixarene skeleton can endow AuNPs with new physicochemical and optical properties crucial for applications ranging from sensing[27,28] to cancer diagnosis and therapy.[29] The calixarene coating can provide AuNPs with (i) enhanced stability and dispersibility in physiological media,[29] (ii) an "active" protecting layer for controlling bioconjugation density,[28] (iii) a receptor layer promoting assembly and networking[30] or (iv) a cluster of ligands for more specific and effective cancer cell targeting.[31]

Different approaches have been tuned for the preparation of calixarene-coated AuNPs.[29] They include postsynthesis approaches in which calixarene derivatives bind preformed AuNPs (e.g., by thiol[32] or diazonium[33] groups, or interdigitation of aliphatic chains[31]) and direct synthesis ones in which Au ions are reduced in the presence of calixarene derivatives that act as stabilizing and/or reducing agents.[32,34] It has been demonstrated that self-assembling materials are good nanoreactors for the formation of AuNPs from Au ions.[35] To the best of our knowledge, only one example of micellar nanoassembly of a cysteinyl-calix[4]arene derivative has been reported in the literature as a template for the preparation of calixarene-coated AuNPs.[36]

AuNPs coated with calixarene-bearing choline groups might be promising candidates for PTT applications. Micellar aggregates of a choline-calix[4]arene conjugate showed no significant toxicity on normal cells[24,37,38] and gene[37] and drug[38,39] delivery properties in in vitro and in vivo experiments. The choline units by binding choline-transporters overexpressed on the surface of cancer cells (ovary, breast, prostate, melanoma, kidney, and colon)[40] might deliver the covered AuNPs to target cells. As a support, AuNPs functionalized with thiocholine showed increased uptake in a human prostate tumor model and decreased intrahepatic accumulation compared with unmodified AuNPs.[41]

Here, we report an unprecedented approach to prepare novel calixarene-coated gold nanoparticles (CholCalix-AuNPs) using a polycationic amphiphilic choline-calix[4]arene derivative (CholCalix) forming micelles and NADH, known to reduce the Au^{3+} ion to AuNPs[42] (Scheme 1A). CholCalix-AuNPs were characterized for structure and optical properties using different techniques including UV−vis and Raman spectroscopies, dynamic light scattering (DLS), and atomic force microscopy (AFM). The NIR-induced photothermal effect for CholCalix-AuNPs was widely investigated (Scheme 1B). A mechanism, supported by molecular modeling simulations, for the formation of CholCalix-AuNPs is proposed. For comparison purposes, the same preparation method was carried out on a micellar polyanionic p-sulfonato-calix[4]arene derivative (SC4OC6)[43] and cationic cetyltrimethyl ammonium bromide (CTAB) micelles lacking the macrocyclic structure. The NIR-light-triggered anticancer effect of CholCalix-AuNPs was tested against a human breast cancer cell line (MDA-MB 231) (Scheme 1C). MTT experiments were performed in comparison to doxorubicin, selected as a model of a highly effective anticancer drug.

■ EXPERIMENTAL SECTION

Materials and Methods. All reagents were purchased from Sigma-Aldrich and used without purification. Materials used for biological tests are described in the appropriate paragraph.

Preparation of CholCalix. CholCalix was prepared according to the procedure depicted in Scheme S1. In brief, commercial p-H-calix[4]arene was blocked in a cone conformation by functionalization of the phenolic hydroxyl groups (lower rim) by C12 alkyl chains.[37] Formyl groups were introduced at the para position of the calixarene aromatic rings (upper rim) and reduced to alcohol groups that were converted to chloromethyl groups.[44] As previously reported,[38] the tetrachloromethyl-O-dodecyl calix[4]arene[44] (2 g, 1.56 mmol) was dissolved in THF (30 mL) and N,N-dimethylethanolamine (0.75 mL, 7.4 mmol) in THF (7.5 mL) was added. The reaction mixture was stirred and refluxed for 24 h. After cooling, the suspension was centrifuged at 4000 rpm for 5 min. The precipitate was washed with THF (20 mL) and then with acetonitrile (4 × 10 mL) by repeated

centrifugation (4000 rpm, 5 min) and removal of the solvent. The precipitate was dried under vacuum to give a white powder (2.1 g, 80% yield). The obtained CholCalix (MW 1648.2 for $C_{96}H_{168}Cl_4N_4O_8$) was characterized by NMR spectroscopy (Figure S1).

Preparation of CholCalix-AuNPs. An aliquot of 18 μL of $HAuCl_4$ (5×10^{-2} M) was added to a micellar dispersion of CholCalix 0.0176 g in 1 mL of PBS under continuous stirring. To an aliquot (500 μL) of the resulting yellow solution of $CholCalix/AuCl_4^-$ was added a volume of 1150 μL of purified citrate AuNPs seeds (150 μL of purified citrate AuNPs was dispersed in 1 mL of Milli-Q deionized water). After stirring, to the resulting solution, 100 μL of NADH (12 mM) was added and heated to 70 °C for 70 min. The final concentrations were 2×10^{-3} M for CholCalix and 690 μM for NADH. The UV−vis−NIR spectra were recorded over time. The resulting dispersion was purified by dialysis using Milli-Q water through a dialysis membrane (6−8 KDa cutoff) for 46 h.

A similar procedure was used to prepare the CholCalix-AuNP dispersion in water starting from a solution of CholCalix (0.0176 g) in 1 mL of Milli-Q deionized water.

Preparation of p-SulfonatoCalix-AuNPs. The amphiphilic p-sulfonato-calix[4]arene bearing hexyl aliphatic chains at the calixarene lower rim (SC4OC6) were prepared according to the procedure reported in the literature.[43] Briefly, to a solution of SC4OH (1.0 g, 1.3 mmol) in water (5 mL) and DMSO (20 mL), NaOH (1.0 g, 25 mmol) and 1-bromohexane (4 mL, 29 mmol) were added. The mixture was stirred at 50 °C for 24 h. After cooling, MeOH was added to obtain a precipitate that was collected by filtration. The solid was dissolved in water (5 mL) and was precipitated again by the addition of EtOH (three times). Then, an aliquot of 18 μL of $HAuCl_4$ (5×10^{-2} M) was added to a micellar dispersion of SC4OC6 (0.0124 g) in 1 mL of Milli-Q deionized water under continuous stirring. To an aliquot (500 μL) of the resulting yellow solution of $SC4OC6/AuCl_4^-$ was added a volume of 1150 μL of purified citrate AuNP seeds (150 μL of purified citrate AuNPs was dispersed in 1 mL of Milli-Q deionized water). After stirring, to the resulting solution was added 100 μL of 12 mM NADH and heated to 70 °C for 70 min. The final concentrations were 3×10^{-3} M for SC4OC6 and 690 μM for NADH. The UV−vis−NIR spectra were recorded over time. The resulting dispersion was purified by dialysis using Milli-Q water through a dialysis membrane (6−8 KDa cutoff) for 46 h.

Preparation of CTAB-AuNPs. An aliquot of 18 μL of $HAuCl_4$ (5×10^{-2} M) was added to a micellar dispersion of 3.7×10^{-2} M of CTAB (0.0135 g in 1 mL of Milli-Q deionized water) under continuous stirring. To an aliquot (500 μL) of the resulting orange dispersion of $CTAB/AuCl_4^-$ was added a volume of 1150 μL of purified citrate AuNP seeds (150 μL of purified citrate AuNPs was dispersed in 1 mL of Milli-Q deionized water). After stirring, to the resulting solution was added 100 μL of NADH (12 mM) and heated to 70 °C for 70 min. The final concentrations were 1×10^{-2} M for CTAB and 690 μM for NADH.

Biological Evaluation. *Cell Culture and Treatments.* Experiments were conducted on the human triple negative breast cancer cell line MDA-MB 231 (HTB-26 ATCC, Rockville, MD). Cells were cultured in Dulbecco's modified Eagle's medium (DMEM) high glucose (HG) supplemented with 10% FBS and 1% penicillin−streptomycin and maintained at 37 °C and 5% CO_2. Cells were treated for 24 h with CholCalix (1 nM to 0.01 mM) and CholCalix-AuNP (2 nM to 0.02 mM) with or without laser radiation; in particular, each well was irradiated at λ = 808 nm for 5 min. Cells were also treated with doxorubicin for 24 h at different concentrations (0.025 μM to 0.025 mM).

Cell Viability Assay. To evaluate cell viability, cells were seeded into 96-well plates at a density of 7.0×10^3 cells/well in 100 μL of a culture medium. After a 24 h treatment, 100 μL of 0.25 mg/mL 3-(4, 5-dimethylthiazol-2-yl)-2, 5-diphenyltetrazolium bromide (MTT) (ACROS Organics- Antwerp, Belgium) solution was added to each well, and cells were incubated for 2 h at 37 °C and 5% CO_2. After incubation, the supernatant was removed and 100 μL of DMSO was added to each well to dissolve formazan salts produced by active

mitochondria. The amount of formazan is proportionate to the number of viable cells in the sample. Ultimately, absorbance (OD) was measured in a microplate reader (Biotek Synergy-HT, Winooski, VT) at $\lambda = 570$ nm. A minimum of three replicate wells was used for each group, and at least two separate experiments were conducted. Results are expressed as mean ± SEM.

Statistical Analysis. Statistical analysis was performed by one-way ANOVA. The honestly significant difference (HSD) method was used as a post hoc test when ANOVA reported statistically significant differences to evaluate the group differences.

Computational Methods. The interaction between CholCalix and gold nanoparticles was evaluated applying the OPLS all-atom force field (OPLS-AA) parametrization through Gromacs 2022 software.[45,46] The Build Nanostructure tool included in Material Studio (MS) software was used to build the gold nanoparticle (AuNP) with a diameter of 3.5 nm. Eight molecules of CholCalix surrounded the AuNP in two different orientations: the CholCalix upper rim facing the AuNP (choline group facing the metal surface) and CholCalix lower rim interacting with AuNP (C12 chain facing the metal surface). The systems were then placed in a box of 15 nm × 15 nm × 7.5 nm and solvated by adding water molecules simulated with TIP3P FF (Figure S2). To investigate the aggregation of CholCalix-AuNPs in a solvent, a model consisting of three units was built (Figure S3).

In all simulations, geometry optimization was performed using the conjugated gradient method, convergence criteria were set to 0.01 kcal mol^{-1}, and molecular dynamics (MD) simulations were run under the periodic boundary condition in the NPT ensemble at $T = 300$ K and $P = 1$ atm (Berendsen barostat, coupling constant = 0.1 ps). The particle-mesh Ewald method was employed to account for the long-range electrostatic interactions with a cutoff distance of 1.5 nm; a time step of 1 fs was chosen to integrate the equation of motion. To simulate the solvated systems, we adopted an equilibration procedure that consists of optimization (20.000 steepest descent steps) of the whole system followed by 50 ns MD of the solvent (solute fixed) and finally a further 400 ns MD was performed removing all of the constraints, and coordinates of the last 200 ns were stored for analysis.[47] During this time, ten structures were randomly sampled for each simulated system and optimized. The energy of interaction between AuNP and calixarene (ΔE_{int}) is calculated as follows

$$\Delta E_{\text{int}} = E_{\text{AuNP}-8x\_\text{calix-water}} - (E_{\text{AuNP}} + 8 \times E_{\text{calix}} + E_{\text{water}}) \quad (1)$$

where E_{AuNP}, E_{calix}, and E_{water} represent the optimized values of potential energy of AuNP, calixarene, and solvent in the bulk. Coherently for the aggregate system, the interaction energy is defined by

$$\Delta E_{\text{int-aggr}} = E_{3x\_\text{AuNP}-8x\_\text{calix-water}} - (3 \times E_{\text{AuNP}} + 8 \times E_{\text{calix}} + E_{\text{water}})$$

Finally, the structural evolution of the aggregate was investigated using the radius of gyration R_g, which is defined as

$$R_g^2 = \frac{\sum_{i=1}^{N} m_i s_i^2}{\sum_{i=1}^{N} m_i}$$

where N is the total number of atoms and s_i is the distance of the atom of index i and mass m_i to the center of mass.

RESULTS AND DISCUSSION

Design, Synthesis, and Characterization of CholCalix-AuNPs. AuNPs are synthesized by reducing Au ions that congregate to form crystals that aggregate to form nanoparticles. Spatial confinement and Au reduction within a chemical template such as a macrocyclic cavity[48,49] or supramolecular self-assembled constructs[50] are effective methods for controlling the formation and size of AuNPs.

The opportune functionalization of the upper rim of a calix[4]arene skeleton blocked in a cone conformation can provide a cage where AuNPs can be formed with a controlled size.[36] It is also known that AuCl$_4^-$ anions can establish interactions with the positively charged ammonium groups of hydrophilic choline chloride functionality by the ion-exchange reaction, and the subsequent addition of a reductant (NaBH$_4$, sodium citrate) can convert the Au ions to AuNPs. Using this approach, AuNPs were built on phosphatidylcholine[51] and on choline chloride functionalized graphene oxide[52] or a glassy carbon electrode.[53]

On that basis, CholCalix bearing choline chloride groups at the upper rim of a calix[4]arene scaffold blocked in a cone conformation by the functionalization of the lower rim phenol groups with dodecyl aliphatic chains (Scheme S1) possesses the requisites to be a template for the preparation of CholCalix-coated AuNPs. CholCalix offers both an electron-rich cavity decorated with choline chloride groups and the property to spontaneously self-assemble in cationic micelles.[37,38,54] To prepare CholCalix-AuNPs, we used a biosynthetic approach based on NADH-dependent Au^{3+} reduction, a method never used for the preparation of calixarene-coated gold nanostructures. The NADH coenzyme alone can reduce the Au^{3+} ion to AuNPs and produce uniformly spherical plasmonic nanoparticles with small sizes (<10 nm diameter).[42]

The possible pathway for the formation of CholCalix-AuNPs is depicted in Figure 1. The addition of AuCl$_4^-$ to the micellar
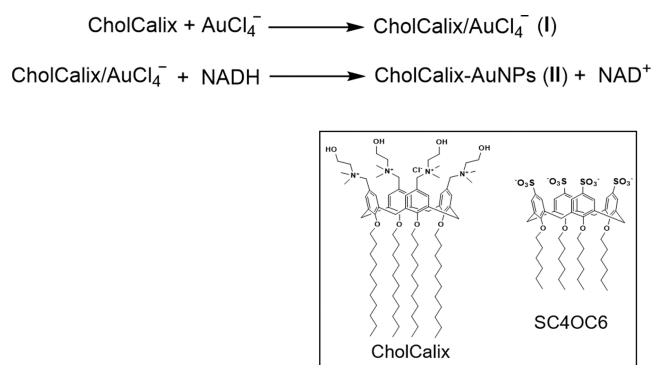

Figure 1. Synthetic pathway for CholCalix-AuNP preparation, and molecular structures of CholCalix and SC4OC6.

CholCalix changes the solution color from colorless to light yellow (Figure 2). The UV−vis spectrum of the solution shows the appearance of an intense optical absorption centered at 468 nm (Figure 2). This band is ascribable to the formation of CholCalix/AuCl$_4^-$ (I) in which the cholinium cationic polar head groups −N$^+$(CH$_3$)$_2$(CH$_2$OH) provide a uniform positively charged surface with a density suitable to establish interactions with AuCl$_4^-$. Upon heating at 70 °C and in the presence of NADH, the intermediate I was rapidly converted to CholCalix-AuNPs (II) (Figure 1), in which AuNPs are formed on the CholCalix micelle surface.

As a confirmation of the above-cited pathway, kinetic studies showed a decrease of both the absorption bands of NADH (340 nm) and CholCalix/AuCl$_4^-$ (I) (468 nm) with the simultaneous increase of an absorption band centered at 540−550 nm (Figure 2) related to the formation of CholCalix-AuNPs (II) (Figure 1). The changes of the UV−vis−NIR optical absorption spectra recorded during the synthesis of
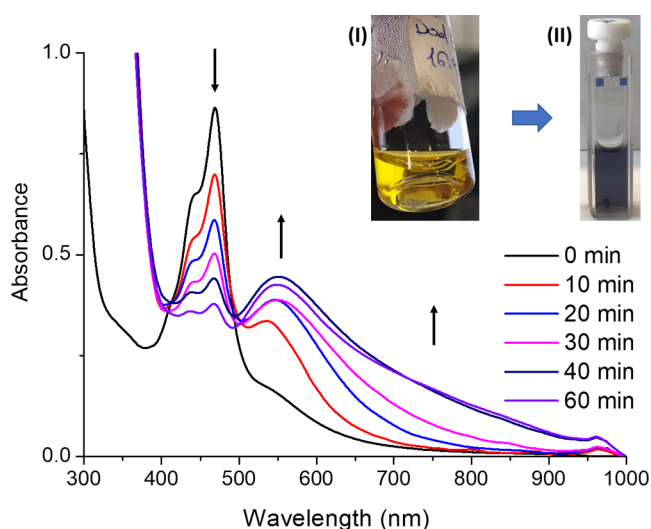
Figure 2. Formation of CholCalix-AuNPs in PBS medium: optical absorption changes over time (0, 10, 20, 30, 40, and 60 min) and inset: change of the solution coloration from yellow (CholCalix/ AuCl$_4^-$ (I)) to blue (CholCalix-AuNPs (II)).

CholCalix-AuNPs (II) also showed the presence of absorption at 600−850 nm (Figure 2). This latter can be the result of multiple scattering and plasmon interactions due to agglomeration phenomena. The formation of AuNPs on the shell of micelles and crosslinked micelles is not unusual.[55] Aggregation phenomena also agree with the previously demonstrated tendency of CholCalix to form aggregates of micelles[38] and a nanohydrogel at higher concentrations and in the presence of curcumin.[39] Therefore, hydrogen bonding involving the choline OH groups and the solvent, interaction of the choline quaternary ammonium groups with colloidal gold, interdigitation of the hydrophobic alkyl chains of CholCalix, and adhesion of gold nanoparticles to each other could lead to the formation of larger agglomerates responsible for the blue coloration of the colloidal solution (Figure 2).

The observed optical behavior is well known in the literature. When AuNPs aggregate, the interaction of locally adjacent Au nanostructures promotes the red shifts of their LSPR band to longer wavelengths.[56,57] This LSPR shift effect is commonly used in colorimetric biosensing.[58−60]

We observed that the solvent affects the aggregation of CholCalix, and larger nanostructures with narrow polydispersity are formed in the presence of salts compared to pure water in which smaller and more polydisperse nanostructures appeared.[24,54] When CholCalix-AuNPs were prepared in deionized water, analogous to the preparation in PBS, the absorption spectrum of the solution showed an absorption band at about 560 nm and a broad band at wavelengths above 650 nm (Figure S4). Dynamic light scattering (DLS) measurements revealed in water the presence of two main nanostructures with the mean hydrodynamic diameters centered at 7 ± 2 nm (10% vol) and 103 ± 10 nm (90% vol) related to single micelles and micelle aggregates, respectively. In PBS, where the aggregation between micelles is more favored, a main population with the mean hydrodynamic diameter centered at 130 ± 5 nm (85% vol) was instead observed. The Z-potential investigation reported for both experiments a positive charge ($+59.8 \pm 1.1$ mV in water and $+28.9 \pm 0.757$ mV in PBS), in agreement with the presence of choline head groups on the surface of the nanoaggregates.

Additionally, evidence of the mechanism proposed in Figure 1 was derived from experiments performed at different CholCalix and NADH amounts. A red shift of the LSPR band from 527 to 564 nm was observed with the increase of the CholCalix concentration from 0.2×10^{-5} to 2×10^{-3} M. At higher CholCalix concentrations, the formation of an additional LSPR band at wavelength above 650 nm (Figure S5) was observed. Similarly, on increasing the NADH concentration from 60 to 690 μM, a gradual increase of the optical absorption at wavelength above 650 nm occurred (Figure S6). These data corroborate the proposed mechanism, where the reducing agent (NADH) promotes Au nanostructure formation in the presence of CholCalix (II-red, λ 540−550 nm). On increasing the concentration of CholCalix, due to its self-assembling nature, larger CholCalix-AuNP aggregates are formed (aggregates of II-blue, λ 600−950 nm). Furthermore, to support the proposed mechanism, experiments were conducted in the absence of CholCalix (Figure S7), and in the absence of CholCalix, NADH, and AuNPs seeds (Figure S8).

Analogous to other AuNPs, the CholCalix organic covering confers dispersibility and stability to the water-insoluble and self-aggregating gold nanoparticles. Absence of a precipitate in
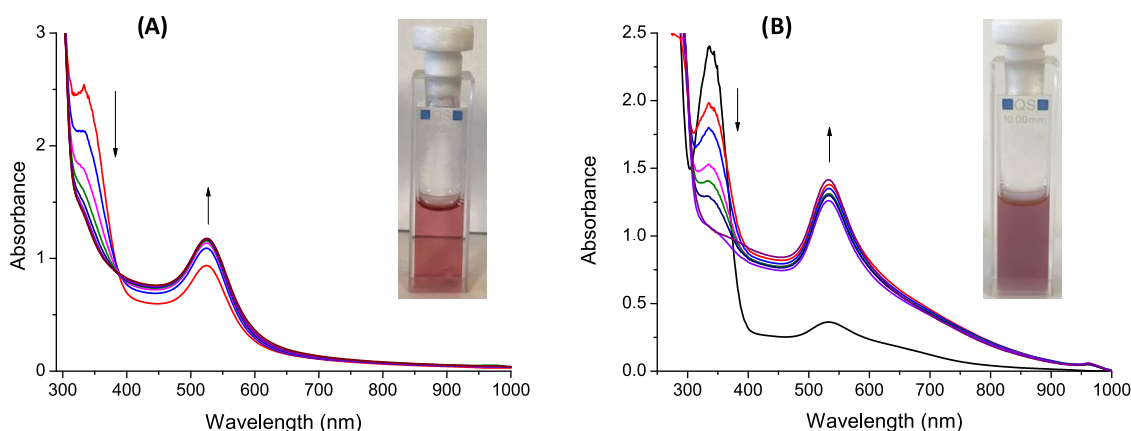

Figure 3. UV−vis spectra for the formation of SC4OC6-Au nanostructures (A) and CTBA-Au nanostructures (B), and pictures of the colored solutions.

water and PBS after weeks from the preparation was observed along with dispersibility in water, PBS, and cell culture medium. Spectroscopically, investigations performed before and after photothermal experiments (10 cycles, CW laser 808 nm) did not report any appreciable change in the absorption spectra of CholCalix-AuNPs (Figure S9).

To better understand the influence of micellar aggregation on Au nanostructure formation, additional experiments were conducted on two amphiphilic compounds, forming micelles with a very low tendency to further aggregation. We selected a *p*-sulfonato-calix[4]arene derivative (SC4OC6), bearing sulfonate groups at the calix[4]arene upper rim and aliphatic hexyl chains at the lower rim[43] (Figure S1), that assembles in negatively charged micelles[61] and cetyltrimethyl ammonium bromide (CTBA) that forms cationic micelles known to stabilize the Au nanorod citrate by forming a stable bilayer with the cationic head groups exposed to the outside.[60,62]

The optical absorption changes for SC4OC6-AuNP formation (SC4OC6, 2×10^{-3} M) in water revealed the formation of nanostructures with the LSPR centered at 525 nm (Figure 3A). The decrease of the NADH absorption band at 340 nm also confirmed for SC4OC6-AuNPs a mechanism like the one proposed in Figure 1. No important absorption at wavelengths above 650 nm indicated that no further aggregation occurs. Figure S10 illustrates the optical absorption spectra for the preparation of SC4OC6-Au nanostructures without Au-seeds. Similarly, in the presence of CTAB (1×10^{-2} M), the optical absorption changes reported in Figure 3B revealed the formation of CTAB-Au nanostructures with the LSPR band centered at 533 nm, with a slight absorption above 650 nm, because no significant formation of aggregates of micelles occurs.

Raman measurements for the CholCalix-Au nanostructures showed relevant differences in the spectral region around 1400 cm^{-1} with respect to CholCalix. In particular, as shown in Figure 4, the amplitude of the band peaked at 1442.5 cm^{-1}, associated with the bending vibration of CH$_2$, features a relative amplitude lower than the nearby bands, suggesting that some modifications have occurred due to the interaction of the CH$_2$ group with the Au nanoparticle surface, or among them. A similar effect was evident in the spectral region around 2850 cm^{-1}. An analogous study for SC4OC6 has been reported in

the supplementary information (Figure S11); also, in this case, interactions involving CH$_2$ groups occur during SC4OC6-AuNP formation.

AFM measurements of CholCalix-AuNPs deposited on the MICA substrate showed both micelles and micelle aggregates were clearly recognizable (Figure 5A). As shown, single micelles have diameters of a few nanometers. Large structures (size range 50−200 nm) detected by AFM analysis could be related to the further aggregation of CholCalix-AuNPs.

To obtain a reliable quantitative estimation of micelle size, a statistical analysis of their diameters was performed. The diameters of the single micelles were estimated by evaluating the height from the extracted profile, and the size distribution obtained with this procedure is reported in Figure 5A (inset). As shown, the diameters of CholCalix micelles fall in the range of 3.5 ± 2 nm, in line with the hydrodynamic size estimated by DLS measurements. In Figure 5B,C, representative cross sections of micelles with sizes 2.5 and 6.5 nm are reported for comparison. The size of the CholCalix-AuNPs (8 nm) was also found to agree with the size estimation obtained with DLS.

It can be assumed that during the synthesis of gold nanoparticles in the calixarene micelles, the particles would grow through intermicellar exchange to a size of about 8 nm in diameter and then agglomerate. Upon agglomeration, further growth would be hindered as the intermicellar exchange is slowed down or prevented. AFM measurements showing particles of 2−8 nm in diameter forming small clusters corroborated this hypothesis.

AFM studies performed on SC4OC6-AuNPs showed nanostructures with diameters in the range of 2 ± 1 nm (Figures S12-14). Smaller size and size distribution were observed for SC4OC6-AuNPs with respect to CholCalix-AuNPs, in agreement with the low tendency of SC4OC6 to form aggregates of micelles.

Molecular Modeling. Geometry optimization clearly suggested that the formation of the system with CholCalix molecules surrounding a single gold nanoparticle with the choline group facing the gold nanoparticle is the most energetically favorable. Indeed, a binding energy (ΔE_{int}) average value of −32.9 kcal mol^{-1} was obtained. In contrast to the CholCalix-AuNP (II) system with CholCalix molecules surrounding gold nanoparticles with the C12 chain facing the metal surface, a significantly higher binding energy with an average value of −13.6 kcal mol^{-1} was calculated. The main contribution to the physisorption energy for the CholCalix-AuNPs (II) system is due to the electrostatic forces between the choline quaternary ammonium cation of CholCalix and the gold surface; alkyl chains are shortened, thus reducing the interaction with the solvent molecules (Figure 6A).

Further investigations were carried out to evaluate the CholCalix-AuNP (II) aggregation. In detail, three units of CholCalix-AuNPs (II) were placed at an initial distance of 6.72, 7.10, and 6.14 nm (Figure S15); hence, molecular dynamics simulations were performed. The binding energy evaluated after optimization geometry showed for the aggregate structure an $\Delta E_{int-aggr}$ average value of about −18.5 kcal mol^{-1} to indicate an additional stabilization due to the CholCalix-AuNP (II) aggregation process (Figure 6B). Moreover, the distances between the AuNP center are reduced during the simulations and, in this case, the alkyl chain at the lower rim seems to play a significant role in the aggregation; van der Waals forces promote interactions between these hydrophobic moieties, further reducing the extent of the
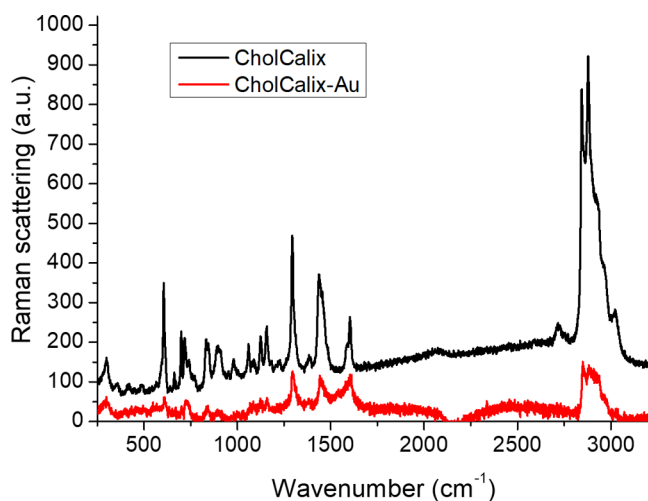

Figure 4. Raman spectra for CholCalix-AuNPs (black line) and CholCalix reference spectrum (red line).
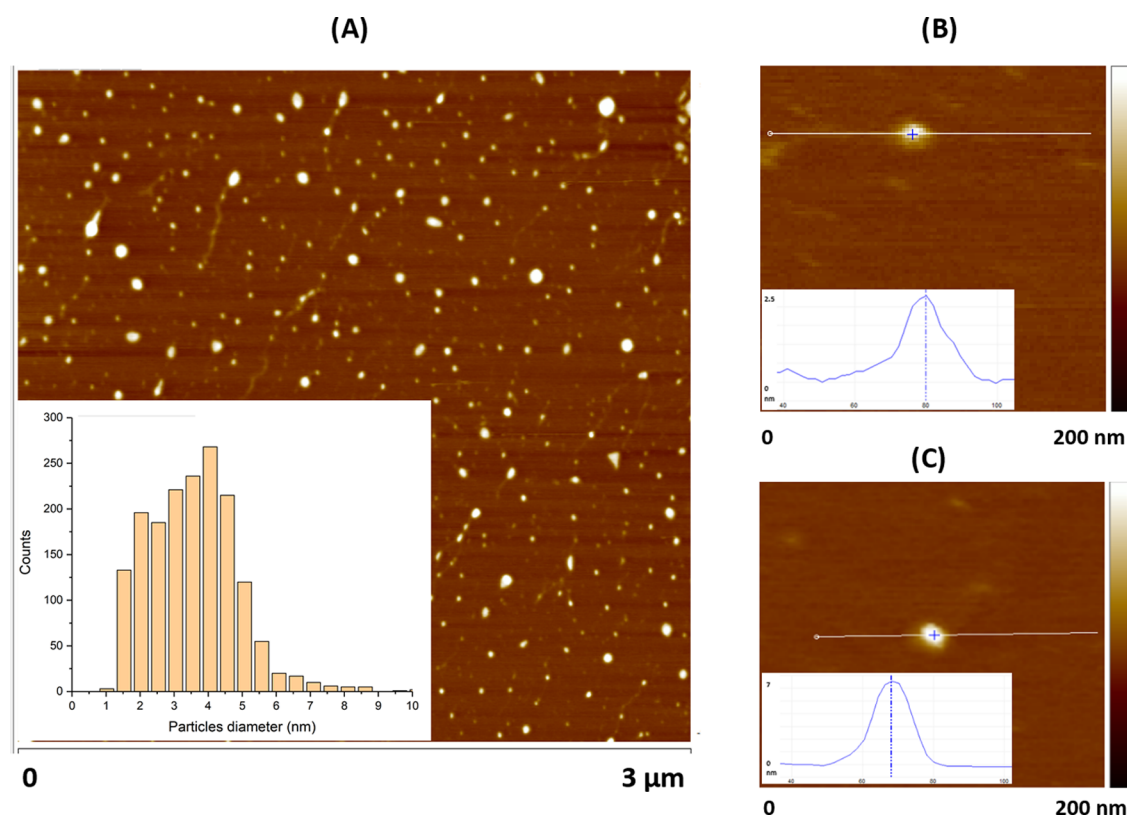
Figure 5. Representative AFM images obtained for CholCalix-AuNPs on MICA substrate. (A) Full scan analysis, 3 μm × 3 μm (inset, size distribution for CholCalix-AuNP). (B) Cross sections for CholCalix-AuNPs. (C) Cross sections for CholCalix-AuNP aggregates.
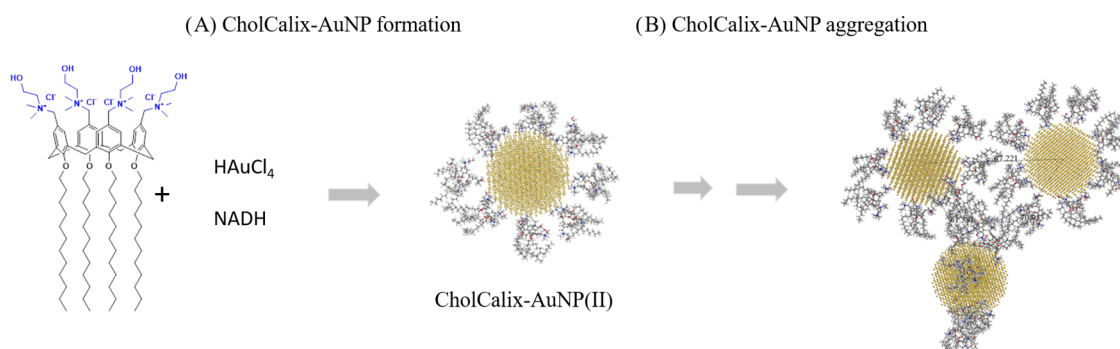

Figure 6. Modeling investigation: (A) CholCalix-AuNP (II) formation process (stabilization binding energy—32.9 Kcal mol^{-1}) and (B) CholCalix-AuNP aggregation process (stabilization binding energy—18.5 Kcal mol^{-1}).

hydrophobic surface, as widely reported in the literature.[62] According to these findings, we observed that the radius of gyration decreased during MD simulation, as shown in Figure 7.

In summary, it is conceivable that in the formation of CholCalix-AuNP nanostructures the following events occur: (1) choline groups establish interactions with the Au surface, as supported by the lower energy found in comparison with the alkyl chain−Au interaction in molecular modeling simulations; (2) the alkyl chains of CholCalix establish hydrophobic interactions among them to form superior order nano-aggregates as evidenced by UV−vis, Raman, and DLS analyses; and (3) interdigitation of the exterior hydrophobic chains with CholCalix molecules can provide a bilayer in which the polar head choline groups provide the AuNPs with an overall positive surface charge, as revealed by ζ potential measure-

ments and water solubility in the absence of precipitation phenomena.

■ PHOTOTHERMAL EXPERIMENTS

Photothermal metal nanomaterials with LSPR absorption are the best applicants for photothermal therapy. As evident in Figure 2, the CholCalix-AuNPs show two main optical absorption bands centered in the visible and NIR regions. The absorption intensity at 808 nm is high enough to lead to a good photothermal conversion efficiency (η), which was measured by exposing various amounts of CholCalix-AuNPs to the laser source (808 nm) by following a standard procedure (SI).

Figure 8 reports the temperature changes, monitored by a thermo-camera, for an aqueous dispersion of CholCalix-AuNPs (100 μL, 0.5 mM, Abs$_{808nm}$ = 0.19 in a glass tube) (Figure 8A)
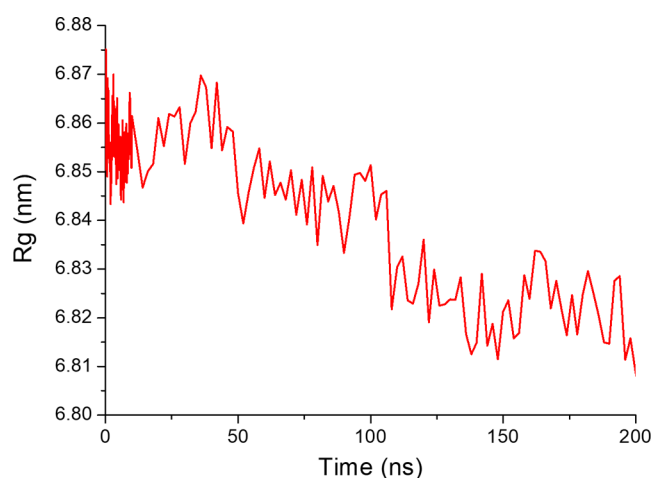
Figure 7. Time evolution of the radius of gyration (Rg) for CholCalix-AuNPs (II).

and for a 96-well plate containing different amounts of CholCalix-Au nanostructures (100 μL, 0 M, 20 μM, 0.2 mM, 0.5 mM, 1 mM, and 2 mM concentrations) (Figure 8B). All samples were continuously exposed to a laser source (808 nm, power density 61.1/cm^2), and when the temperature of the system reached a steady state (T_{max} 44.2 °C), the laser was shut off. The temperature of the samples increased, from 0 to 8.5, 29.8, and 39 °C, by increasing the amount of the CholCalix-Au nanostructures. Figure 8C illustrates representative thermograph images recorded by the thermo-camera during the photothermal experiments in the tube with the CholCalix-AuNP solution (0.5 mM). Figure 8D depicts the thermograph images recorded by the thermo-camera during the photothermal experiments in a 96-well plate. Temperature increases of about 7.1 °C are evident in the well exposed to the 808 nm light and containing the CholCalix-AuNP solution (20 μM).

The temperature change during cooling was monitored to confirm the rate of heat transfer of the system. The time constant τs was calculated from the graph reported in Figure S16 to be 100.4 ± 1.6 s. Based on the data, the light-driven photothermal conversion efficiency (η) of the CholCalix-Au
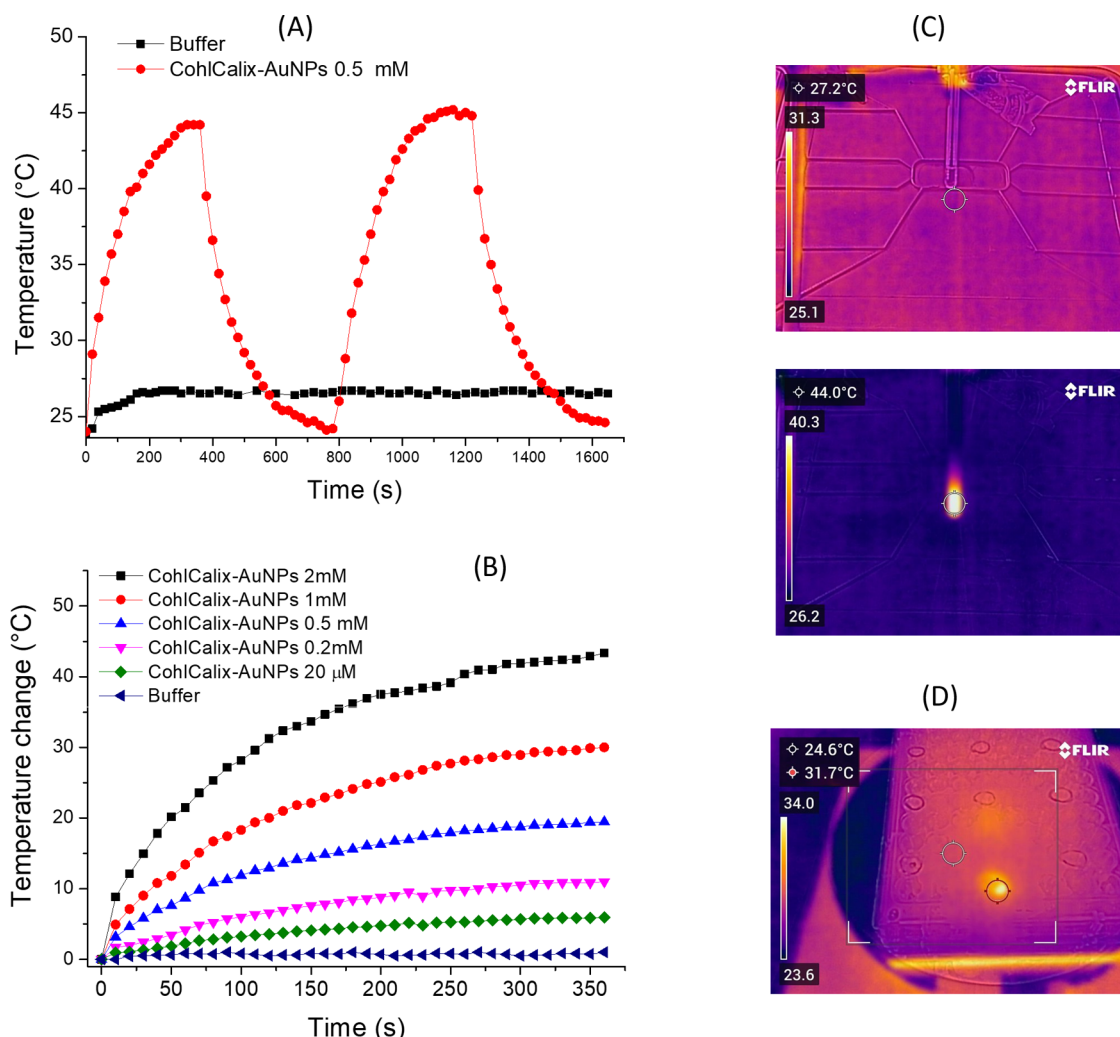

Figure 8. Photothermal experiments for CholCalix-Au (II) nanostructure dispersion. (A) Photothermal heating−cooling cycles of CholCalix-AuNP nanostructure PBS dispersion, volume 100 μL, Abs$_{808nm}$ = 0.19 in a glass tube. (B) Photothermal effect of CholCalix-Au nanostructures at various amounts (0, 20 μM, 0.2 mM, 0.5 mM 1 mM, and 2 mM) in a 96-well plate (volume 100 μL). (C) Representative thermographs during photothermal experiments in a glass tube and (D) representative thermographs during the photothermal experiments a 96-well plate (CholCalix-AuNPs 20 μM).
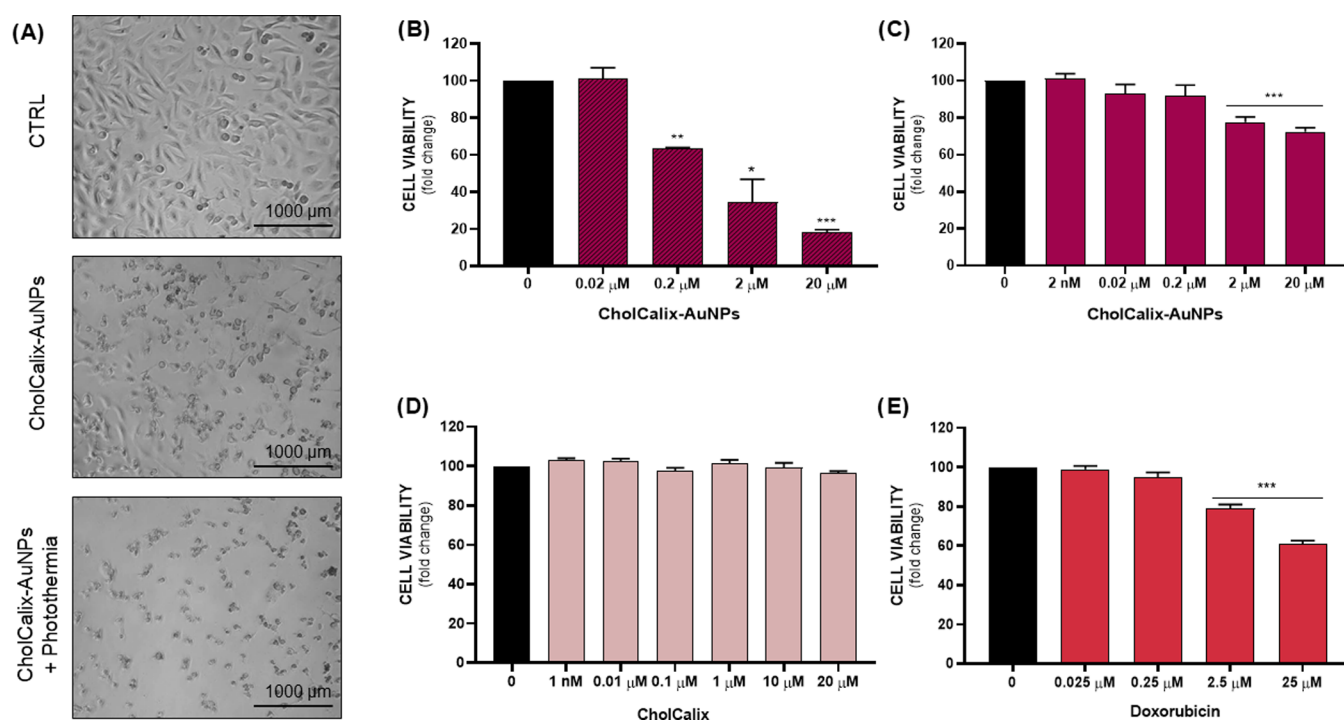
Figure 9. (A) Representative images of untreated and treated cells (max concentration: 20 μM). (B) Assessment of CholCalix-AuNPs combined with photothermic treatment (808 nm, 5 min/well), effect on MDA-MB 231 cell viability (*$p < 0.05$; **$p < 0.005$; ***$p < 0.0005$ vs CTRL (0)). (C, D) Evaluation of CholCalix-AuNPs and CholCalix effect at different concentrations on MDA-MB 231 cell viability following 24 h of treatment (***$p < 0.0005$ vs CTRL (0)). (E) Evaluation of doxorubicin cytotoxicity on the MDA-MB 231 cell line (***$p < 0.0005$ vs CTRL (0)).

nanostructures was calculated to be 38.7%, which is high enough for an efficient photothermal anticancer therapy.

CELL VIABILITY TEST

CholCalix-AuNPs appear promising candidates for application in PTT. The choline ligands by binding choline-transporters overexpressed on the surface of cancer cells[40] might deliver the covered AuNPs to cancer cells. The gene[37] and drug delivery[38,39] properties of CholCalix micelles were demonstrated along with the increased intratumor uptake of AuNPs functionalized with thiocholine.[41]

Data obtained from the cell viability test performed on an epithelial human breast cancer cell line (MDA-MB 231) showed that the combination of CholCalix-AuNPs and photothermia results in a higher cancer cell mortality. The number of not viable cells increased considerably when the cells were treated with CholCalix-AuNPs and irradiated with NIR light for 5 min. Cell mortality (%) dose−response values of 30, 65, and 80% were observed at concentrations of 0.2, 2.0, and 20 μM CholCalix-AuNPs, respectively (Figure 9A,B).

Differently, a moderate reduction of viable cells (15 and 20%) was observed when the cells were treated with CholCalix-AuNPs without irradiation at concentrations of 2.0 and 20 μM, respectively (Figure 9C). Light exposure without CholCalix-AuNPs did not affect cell viability (data not shown). Additionally, data reported in Figure 9D showed no cytotoxicity on MDA-MB 231 cells after 24 h of incubation with CholCalix (1 nM to 10 μM), highlighting that gold nanoparticles and especially light are crucial for an effective anticancer activity.

The observed modest toxicity on cancer cells, which generally are more sensitive than normal cells,[63] suggest CholCalix-AuNPs as new biofriendly light-responsive agents

for PTT. CholCalix-AuNPs consist of two components CholCalix and AuNP whose biocompatibility singularly has been demonstrated. The biosafety of CholCalix-AuNPs is supported by the insignificant toxicity of CholCalix, proved on other cell lines (HeLa cells,[37] fibroblasts,[24,64] corneal cells,[38] retinal cells[65]) and animal model of psoriasis,[66] and by the known biocompatibility of AuNPs.[67] As an added value, CholCalix offers the potential advantage to target cancer cells while sparing normal cells.

Noteworthy, a comparison study revealed that the irradiated CholCalix-AuNPs exhibit a higher cytotoxic activity than doxorubicin, selected as a model of an effective anticancer drug with a broad spectrum of action. Indeed, MTT assays showed that doxorubicin at 2.5 and 25 μM concentrations caused 20−30% mortality, while irradiated CholCalix-AuNPs (2.0 and 20 μM concentration) induced 65 and 80% mortality on MDA-MB 231 cells.

CONCLUSIONS

For the first time, a choline-calix[4]arene derivative self-assembling in micelles has been investigated as a template for the preparation of water-soluble gold nanostructures decorated with multiple choline ligands for cancer cell targeting. The mechanism proposed for the formation of calixarene-coated AuNPs, corroborated by different techniques and molecular modeling simulations, suggested the formation of small AuNPs in the calix[4]arene-defined cage that, depending on the concentration, further self-assemble in agglomerates absorbing NIR light, a biocompatible and tissue-penetrating light. The calixarene-coated gold nanostructures showed no significant toxicity and, under light irradiation, significantly reduced the viability of breast cancer cells due to a photothermal effect. The biosynthetic method based on the use of NADH as the

Au-ion reducing agent and a calix[4]arene macrocyclic-based micelle as a template for controlling the AuNP size is a promising approach for the fabrication of gold nanostructures for photothermal therapy.

■ ASSOCIATED CONTENT

ⓢ Supporting Information

The Supporting Information is available free of charge at https://pubs.acs.org/doi/10.1021/acsanm.2c04501.

> CholCalix synthesis and ^{1}H-NMR spectrum; preparation and characterization of citrate AuNP seeds; computational models; optical absorption spectra; Au nanostructure formation without CholCalix or without NADH, CholCalix, and Au-seeds; preparation of SC4OC6-AuNPs without Au-seeds; Raman spectra and AFM images of SC4OC6-AuNPs; and photothermal time constant calculation (PDF)

■ AUTHOR INFORMATION

Corresponding Authors

Grazia M. L. Consoli − *CNR-Institute of Biomolecular Chemistry, 95126 Catania, Italy; CIB-Interuniversity Consortium for Biotechnologies U.O. of Catania, 34148 Trieste, Italy;* ⓞ orcid.org/0000-0003-4189-930X; Email: grazia.consoli@icb.cnr.it

Salvatore Petralia − *Department of Drug Science and Health, University of Catania, 95125 Catania, Italy; CIB-Interuniversity Consortium for Biotechnologies U.O. of Catania, 34148 Trieste, Italy;* ⓞ orcid.org/0000-0001-5692-1130; Email: salvatore.petralia@unict.it

Authors

Giuseppe Forte − *Department of Drug Science and Health, University of Catania, 95125 Catania, Italy*

Ludovica Maugeri − *Department of Drug Science and Health, University of Catania, 95125 Catania, Italy;* ⓞ orcid.org/0000-0003-3839-3754

Valeria Consoli − *Department of Drug Science and Health, University of Catania, 95125 Catania, Italy;* ⓞ orcid.org/0000-0001-8961-5818

Valeria Sorrenti − *Department of Drug Science and Health, University of Catania, 95125 Catania, Italy;* ⓞ orcid.org/0000-0002-5973-1495

Luca Vanella − *Department of Drug Science and Health, University of Catania, 95125 Catania, Italy;* ⓞ orcid.org/0000-0002-6314-6029

Gianpiero Buscarino − *Dipartimento di Fisica e Chimica, University of Palermo, Palermo 90133, Italy;* ⓞ orcid.org/0000-0001-8324-6783

Simonpietro Agnello − *Dipartimento di Fisica e Chimica, University of Palermo, Palermo 90133, Italy;* ⓞ orcid.org/0000-0002-0346-8333

Massimo Camarda − *ST-Lab srl, 95126 Catania, Italy*

Giuseppe Granata − *CNR-Institute of Biomolecular Chemistry, 95126 Catania, Italy;* ⓞ orcid.org/0000-0001-9428-3985

Loredana Ferreri − *CNR-Institute of Biomolecular Chemistry, 95126 Catania, Italy*

Complete contact information is available at:
https://pubs.acs.org/10.1021/acsanm.2c04501

Author Contributions

The manuscript was written through contributions of all authors. All authors have given approval to the final version of the manuscript.

Notes

The authors declare no competing financial interest.

■ REFERENCES

(1) Rodríguez, F.; Caruana, P.; De la Fuente, N.; Español, P.; Gámez, M.; Balart, J.; Llurba, E.; Rovira, R.; Ruiz, R.; Martín-Lorente, C.; Corchero, J. L.; Céspedeset, M. V. Nano-Based Approved Pharmaceuticals for Cancer Treatment: Present and Future Challenges. *Biomolecules* **2022**, *12*, No. 784.

(2) Wu, J. The Enhanced Permeability and Retention (EPR) Effect: The Significance of the Concept and Methods to Enhance Its Application. *J. Pers. Med.* **2021**, *11*, No. 771.

(3) Akhtar, M. J.; Ahamed, M.; Alhadlaq, H. A.; Alrokayan, S. A.; Kuma, S. Targeted anticancer therapy: overexpressed receptors and nanotechnology. *Clin. Chim. Acta* **2014**, *436*, 78−92.

(4) Li, L.; Yang, W. W.; Xu, D.-G. Stimuli-responsive nanoscale drug delivery systems for cancer therapy. *J. Drug Targeting* **2019**, *27*, 423−433.

(5) Zhao, L.; Zhang, X.; Wang, X.; et al. Recent advances in selective photothermal therapy of tumor. *J. Nanobiotechnol.* **2021**, *19*, No. 335.

(6) Cao, Y.; Ren, Q.; Hao, R.; Sun, Z. Innovative strategies to boost photothermal therapy at mild temperature mediated by functional nanomaterials. *Mater. Des.* **2022**, *214*, No. 110391.

(7) Zhang, B.; Yu, Q.; Zhang, Y.-M.; Liu, Y. Two-dimensional supramolecular assemblies based on β-cyclodextrin-grafted graphene oxide for mitochondrial dysfunction and photothermal therapy. *Chem. Commun.* **2019**, *55*, 12200−12203.

(8) Zhou, Z.; Jiang, N.; Chen, J.; Zheng, C.; Guo, Y.; Ye, R.; Qi, R.; Shen, J. Selectively down-regulated PD-L1 by albumin-phenformin nanoparticles mediated mitochondrial dysfunction to stimulate tumor-specific immunological response for enhanced mild-temperature photothermal efficacy. *J. Nanobiotechnol.* **2021**, *19*, No. 375.

(9) Petralia, S.; Forte, G.; Aiello, M.; Nocito, G.; Conoci, S. Photothermal-triggered system for oligonucleotides delivery from cationic gold nanorods surface: A molecular dynamic investigation. *Colloids Surf., B* **2021**, *201*, No. 111654.

(10) Chuang, Y.-C.; Lee, H.-L.; Chiou, J.-F.; Lo, L.-W. Recent Advances in Gold Nanomaterials for Photothermal Therapy. *J. Nanotheranostics* **2022**, *3*, 117−131.

(11) Chen, G.; Qian, Y.; Zhang, H.; Ullah, A.; He, X.; Zhou, Z.; Fenniri, H.; Shen, J. Advances in cancer theranostics using organic-inorganic hybrid nanotechnology. *Appl. Mater. Today* **2021**, *23*, No. 101003.

(12) Riley, R. S.; Day, E. S. Gold nanoparticle-mediated photothermal therapy: applications and opportunities for multimodal cancer treatment. *Wiley Interdiscip. Rev.: Nanomed. Nanobiotechnol.* **2017**, *9*, No. 1449.

(13) Vines, J. B.; Yoon, J. H.; Ryu, N. E.; Lim, D. J.; Park, H. Gold Nanoparticles for Photothermal Cancer Therapy. *Front Chem.* **2019**, *7*, No. 167.

(14) Bansal, S. A.; Kumar, V.; Karimi, J.; Singh, A. P.; Kumar, S. Role of Gold Nanoparticles in Advanced Biomedical Applications. *Nanoscale Adv.* **2020**, *2*, 3764−3787.

(15) Kumar, A.; Ma, H.; Zhang, X.; Huang, K.; Jin, S.; Liu, J.; Wei, T.; Cao, W.; Zou, G.; Liang, X.-J. Gold Nanoparticles Functionalized with Therapeutic and Targeted Peptides for Cancer Treatment. *Biomaterials* **2012**, *33*, 1180−1189.

(16) Jazayeri, M. H.; Amani, H.; Pourfatollah, A. A.; Pazoki-Toroudi, H.; Sedighimoghaddam, B. Various Methods of Gold Nanoparticles (GNPs) Conjugation to Antibodies. *Sens. Bio-Sensing Res.* **2016**, *9*, 17–22.

(17) Zhang, C.; Wu, R.; Li, Y.; Zhang, Q.; Yang, J. Programmable Regulation of DNA Conjugation to Gold Nanoparticles via Strand Displacement. *Langmuir* **2017**, *33*, 12285–12290.

(18) Prabhakaran, P.; Kumar, P.; Lim, D.-K. Gold-Polymer Nanocomposites for Future Therapeutic and Tissue Engineering Applications. *Pharmaceutics* **2022**, *14*, No. 70.

(19) Pan, Y.-C.; Hu, X.-Y.; Guo, D.-S. Biomedical Applications of Calixarenes: State of the Art and Perspectives. *Angew. Chem., Int. Ed.* **2021**, *60*, 2768–2794.

(20) Yousaf, A.; Abd Hamid, S.; Bunnori, N. M.; Ishola, A. A. Applications of calixarenes in cancer chemotherapy: facts and perspectives. *Drug Des., Dev. Ther.* **2015**, *9*, 2831–2838.

(21) Yue, Y.-X.; Zhang, Z.; Wang, Z.-H.; Ma, R.; Chen, M.-M.; Ding, F.; Li, H.-B.; Li, J.-J.; Shi, L.; Liu, Y.; Guo, D.-S. Promoting Tumor Accumulation of Anticancer Drugs by Hierarchical Carrying of Exogenous and Endogenous Vehicles. *Small Struct.* **2022**, *3*, No. 2200067.

(22) Xu, L.; Chai, J.; Wang, Y.; Zhao, X.; Guo, D.-S.; Shi, L.; Zhang, Z.; Liu, Y. Calixarene-integrated nano-drug delivery system for tumor-targeted delivery and tracking of anti-cancer drugs in vivo. *Nano Res.* **2022**, *15*, 7295–7303.

(23) Xiong, W.; Qi, L.; Jiang, N.; Zhao, Q.; Chen, L.; Jiang, X.; Li, Y.; Zhou, Z.; Shen, J. Metformin liposome-mediated PD-L1 downregulation for amplifying the photodynamic immunotherapy efficacy. *ACS Appl. Mater. Interfaces* **2021**, *13*, 8026–8041.

(24) Di Bari, I.; Picciotto, R.; Granata, G.; Blanco, A. R.; Consoli, G. M. L.; Sortino, S. A bactericidal calix[4]arene-based nanoconstruct with amplified NO photorelease. *Org. Biomol. Chem.* **2016**, *14*, 8047–8052.

(25) Feng, H.-T.; Li, Y.; Duan, X.; Wang, X.; Qi, C.; Lam, J. W. Y.; Ding, D.; Tang, B. Z. Substitution Activated Precise Photo-theranostics through Supramolecular Assembly of AIEgen and Calixarene. *J. Am. Chem. Soc.* **2020**, *142*, 15966–15974.

(26) Zhang, T.-X.; Hou, X.; Kong, Y.; Yang, F.; Yue, Y.-X.; Shah, M. R.; Li, H.-B.; Huang, F.; Liu, J.; Guo, D.-S. A hypoxia-responsive supramolecular formulation for imaging-guided photothermal therapy. *Theranostics* **2022**, *12*, 396–409.

(27) Li, P.-Y.; Chen, Y.; Chen, C.-H.; Liu, Y. Multi-charged bis(p-calixarene)/pillararene functionalized gold nanoparticles for ultra-sensitive sensing of butyrylcholinesterase. *Soft Matter* **2019**, *15*, 8197–8200.

(28) Retout, M.; Blond, P.; Jabin, I.; Bruylants, G. Ultrastable PEGylated Calixarene-Coated Gold Nanoparticles with a Tunable Bioconjugation Density for Biosensing Applications. *Bioconjugate Chem.* **2021**, *32*, 290–300.

(29) Kongor, A. R.; Mehta, V. A.; Modi, K. M.; Panchal, M. K.; Dey, A. S.; Panchal, U. S.; Jain, V. K. Calix-Based Nanoparticles: A Review. *Top. Curr. Chem.* **2016**, *374*, No. 28.

(30) Ciesa, F.; Plech, A.; Mattioli, C.; Pescatori, L.; Arduini, A.; Pochini, A.; Rossi, F.; Secchi, A. Guest controlled assembly of gold nanoparticles coated with calix[4]arene hosts. *J. Phys. Chem. C* **2010**, *114*, 13601–13607.

(31) Avvakumova, S.; Fezzardi, P.; Pandolfi, L.; Colombo, M.; Sansone, F.; Casnati, A.; Prosperi, D. Gold nanoparticles decorated by clustered multivalent cone-glycocalixarenes actively improve the targeting efficiency toward cancer cells. *Chem. Commun.* **2014**, *50*, 11029–11032.

(32) Ha, J.-M.; Katz, A.; Drapailo, A. B.; Kalchenko, V. I. Mercaptocalixarene-Capped Gold Nanoparticles via Postsynthetic Modification and Direct Synthesis: Effect of Calixarene Cavity-Metal Interactions. *J. Phys. Chem. C* **2009**, *113*, 1137–1142.

(33) Valkenier, H.; Malytskyi, V.; Blond, P.; Retout, M.; Mattiuzzi, A.; Goole, J.; Raussens, V.; Jabin, I.; Bruylants, G. Controlled functionalisation of gold nanoparticles with mixtures of calix[4]arenes revealed by infra-red spectroscopy. *Langmuir* **2017**, *33*, 8253–8259.

(34) Khalid, S.; Parveen, S.; Raza, M.; Sana, S.; Shakil, R.; Muhammad, A.; Malik, I. Calixarene coated gold nanoparticles as a novel therapeutic agent. *Arabian J. Chem.* **2020**, *13*, 3988–3996.

(35) Carrot, G.; Valmalette, J. C.; Plummer, C. J. G.; Scholz, S. M.; Dutta, J.; Hofmann, H.; Hilborn, J. G. Gold nanoparticle synthesis in graft copolymer micelles. *Colloid Polym. Sci.* **1998**, *276*, 853–859.

(36) Fujii, S.; Sakurai, K.; Okobira, T.; Ohta, N.; Takahara, A. Synthesis and characterization of a calix[4]arene amphiphile bearing cysteine and uniform Au nanoparticle formation templated by its four cysteine moieties. *Langmuir* **2013**, *29*, 13666–13675.

(37) Rodik, R. V.; Anthony, A. S.; Kalchenko, V. I.; Melya, Y.; Klymchenko, A. S. Cationic amphiphilic calixarenes to compact DNA into small nanoparticles for gene delivery. *New J. Chem.* **2015**, *39*, 1654–1664.

(38) Granata, G.; Paterniti, I.; Geraci, C.; Cunsolo, F.; Esposito, E.; Cordaro, M.; Blanco, A. R.; Cuzzocrea, S.; Consoli, G. M. L. Potential eye drop based on a calix[4]arene nanoassembly for curcumin delivery: Enhanced drug solubility, stability, and anti-inflammatory effect. *Mol. Pharmaceutics* **2017**, *14*, 1610–1622.

(39) Granata, G.; Petralia, S.; Forte, G.; Conoci, S.; Consoli, G. M. L. Injectable supramolecular nanohydrogel from a micellar self-assembling calix[4]arene derivative and curcumin for a sustained drug release. *Mater. Sci. Eng. C* **2020**, *111*, No. 110842.

(40) Hara, T.; Bansal, A.; DeGrado, T. R. Choline Transporter as a Novel Target for Molecular Imaging of Cancer. *Mol. Imaging* **2006**, *5*, 498–509.

(41) Razzak, R.; Zhou, J.; Yang, X. H.; Pervez, N.; Bédard, E. L. R.; Moore, R. B.; Shaw, A.; Amanie, J.; Roa, W. H. The biodistribution and pharmacokinetic evaluation of choline-bound gold nanoparticles in a human prostate tumor xenograft model. *Clin. Invest. Med.* **2013**, *36*, 133–142.

(42) Baymiller, M.; Huang, F.; Rogelj, S.Rapid one-step synthesis of gold nanoparticles using the ubiquitous coenzyme NADH*Matters*2017 DOI: 10.19185/matters.201705000007.

(43) Jin, T.; Fujii, F.; Sakata, H.; Tamura, M.; Kinjo, M. Amphiphilic p-sulfonatocalix[4]arene-coated CdSe/ZnS quantum dots for the optical detection of the neurotransmitter acetylcholine. *Chem. Commun.* **2005**, *34*, 4300–4302.

(44) Eggers, P. K.; Becker, T.; Melvin, M. K.; Boulos, R. A.; James, E.; Morellini, N.; Harvey, A. R.; Dunlop, S. A.; Fitzgerald, M.; Stubbs, K. A.; Raston, C. L. Composite fluorescent vesicles based on ionic and cationic amphiphilic calix[4]arenes. *RSC Adv.* **2012**, *2*, 6250–6257.

(45) Abraham, M. J.; Murtola, T.; Schulz, R.; Páll, S.; Smith, J. C.; Hess, B.; Lindahl, E. GROMACS: high performance molecular simulations through multi-level parallelism from laptops to super-computers. *Software X* **2015**, *1–2*, 19–25.

(46) Jorgensen, W. L.; Maxwell, D. S.; Tirado-Rives, J. Development and Testing of the OPLS All-Atom Force Field on Conformational Energetics and Properties of Organic Liquids. *J. Am. Chem. Soc.* **1996**, *118*, 11225–11236.

(47) Consiglio, G.; Failla, S.; Fortuna, C. G.; D'Urso, F.; D'Urso, L.; Forte, G. Aggregation of a Zn(II)-salen complex: Theoretical study of structure and spectra. *Comput. Theor. Chem.* **2015**, *1067*, 1–6.

(48) Geng, Y.; Liu, M.; Xue, J.; Xu, P.; Wang, Y.; Shu, L.; Zeng, Q.; Wang, C. A template-confined fabrication of controllable gold nanoparticles based on the two-dimensional nanostructure of macrocycles. *Chem. Commun.* **2015**, *51*, 6820–6823.

(49) Chung, J. W.; Guo, Y.; Kwak, S.-Y.; Priestley, R. D. Understanding and controlling gold nanoparticle formation from a robust self-assembled cyclodextrin solid template. *J. Mater. Chem.* **2012**, *22*, 6017–6026.

(50) Arunagirinathan, M.; Huggins, K.; Schoen, A.; Heilshorn, S. Clathrin Self-Assembly Templates for Gold Nanoparticle Nucleation. *Microscopy Microanal.* **2012**, *18*, 1628–1629.

(51) Mackiewicz, M. R.; Ayres, B. R.; Reed, S. M. Reversible, reagentless solubility changes in phosphatidylcholine-stabilized gold nanoparticles. *Nanotechnology* **2008**, *19*, No. 115607.

(52) Bahrani, S.; Razmi, Z.; Ghaedi, M.; Asfaram, A.; Javadian, H. Ultrasound-accelerated synthesis of gold nanoparticles modified

choline chloride functionalized graphene oxide as a novel sensitive bioelectrochemical sensor: Optimized meloxicam detection using CCD-RSM design and application for human plasma sample. *Ultrason. Sonochem.* **2018**, *42*, 776−786.

(53) Wang, P.; Mai, Z.; Dai, Z.; Li, Y.; Zou, X. Construction of Au nanoparticles on choline chloride modified glassy carbon electrode for sensitive detection of nitrite. *Biosens. Bioelectron.* **2009**, *24*, 3242−3247.

(54) Migliore, R.; Granata, G.; Rivoli, A.; Consoli, G. M. L.; Sgarlata, C. Binding affinity and driving forces for the interaction of calixarene-based micellar aggregates with model antibiotics in neutral aqueous solution. *Front. Chem.* **2021**, *8*, No. 626467.

(55) Sakurai, H.; Mitsuharu, K.Preparation of metal nanoparticles using shell-crosslinked micelle as template. JP2003147418A, 2008.

(56) Wu, S.; Lei, L.; Xia, Y.; Oliver, S.; Chen, X.; Boyer, C.; Nie, Z.; Shi, S. PNIPAM-immobilized gold-nanoparticles with colorimetric temperature-sensing and reusable temperature-switchable catalysis properties. *Polym. Chem.* **2021**, *12*, 6903−6913.

(57) Azzazy, H. M. E.; Mansour, M. M. H.; Samir, T. M.; Franco, R. Gold nanoparticles in the clinical laboratory: principles of preparation and applications. *Clin. Chem. Lab. Med.* **2012**, *50*, 193−209.

(58) Howes, P. D.; Chandrawati, R.; Stevens, M. M. Colloidal nanoparticles as advanced biological sensors. *Science* **2014**, *346*, 1247390−1247391.

(59) Anker, J. N.; Hall, W. P.; Lyandres, O.; Shah, N. C.; Zhao, J.; Van Duyne, R. P. Biosensing with plasmonic nanosensors. *Nat. Mater.* **2008**, *7*, 442−453.

(60) Lim, J.; Lee, N.-E.; Lee, E.; Yoon, S. Surface modification of citrate-capped gold nanoparticles using CTAB micelles. *Bull. Korean Chem. Soc.* **2014**, *35*, 2567−2569.

(61) Basílio, N.; Garcia-Rio, L. Calixarene-based surfactants: Conformational-dependent solvation shells for the alkyl chains. *ChemPhysChem* **2012**, *13*, 2368−2376.

(62) Yoon, J. H.; Park, J. S.; Yoon, S. Time-dependent and symmetry-selective charge-transfer contribution to SERS in gold nanoparticle aggregates. *Langmuir* **2009**, *25*, 12475−12480.

(63) Wang, L.; Zhao, X.; Fu, J.; Xu, W.; Yuan, J. The Role of Tumor Metabolism in Cisplatin Resistance. *Front. Mol. Biosci.* **2021**, *8*, No. 691795.

(64) Ferreri, L.; Consoli, G. M. L.; Clarizia, G.; Zampino, D. C.; Nostro, A.; Granata, G.; Ginestra, G.; Giuffrida, M. L.; Zimbone, S.; Bernardo, P. Novel material based on an antibacterial choline-calixarene nanoassembly embedded in thin films. *J. Mater. Sci.* **2022**, *57*, 20685−20701.

(65) Blanco, R.; Bondì, M. L.; Cavallaro, G.; Consoli, G. M. L.et al.Nanostructured formulations for the delivery of silibinin and other active ingredients for treating ocular diseases. WO055976, 2016.

(66) Filippone, A.; Consoli, G. M. L.; Granata, G.; Casili, G.; Lanza, M.; Ardizzone, A.; Cuzzocrea, S.; Esposito, E.; Paterniti, I. Topical Delivery of Curcumin by Choline-Calix[4]arene-Based Nanohydrogel Improves Its Therapeutic Effect on a Psoriasis Mouse Model. *Int. J. Mol. Sci.* **2020**, *21*, No. 5053.

(67) Kadhim, R. J.; Karsh, E. H.; Taqi, Z. J.; Jabir, M. S. Biocompatibility of gold nanoparticles: *In-vitro* and *In-vivo* study. *Mater. Today: Proc.* **2021**, *42*, 3041−3045.